blood®
Regular Article

Check for updates

PLATELETS AND THROMBOPOIESIS

Enhancer-gene rewiring in the pathogenesis of Quebec platelet disorder

Minggao Liang,[1,2] Asim Soomro,[3] Subia Tasneem,[3] Luis E. Abatti,[4] Azad Alizada,[1,2] Xuefei Yuan,[1,2] Liis Uusküla-Reimand,[1] Lina Antounians,[1,2] Sana Akhtar Alvi,[1] Andrew D. Paterson,[1,5] Georges-Étienne Rivard,[6] Ian C. Scott,[1,2] Jennifer A. Mitchell,[4] Catherine P. M. Hayward,[3,6,7,*] and Michael D. Wilson[1,2,*]

[1]Program in Genetics and Genome Biology, SickKids Research Institute, Toronto, ON, Canada; [2]Department of Molecular Genetics, The University of Toronto, Toronto, ON, Canada; [3]Department of Pathology and Molecular Medicine, McMaster University, Hamilton, ON, Canada; [4]Department of Cell and Systems Biology and [5]Dalla Lana School of Public Health and Institute of Medical Sciences, The University of Toronto, ON, Canada; [6]Hematology/Oncology, Centre Hospitalier Universitaire Sainte-Justine, Montreal, QC, Canada; and [7]Department of Medicine, McMaster University, Hamilton, ON, Canada

KEY POINTS

- **Duplication of *PLAU* in QPD disrupts genome architecture and rewires enhancer-gene interactions, causing cell type–specific overexpression.**

Quebec platelet disorder (QPD) is an autosomal dominant bleeding disorder with a unique, platelet-dependent, gain-of-function defect in fibrinolysis, without systemic fibrinolysis. The hallmark feature of QPD is a >100-fold overexpression of *PLAU*, specifically in megakaryocytes. This overexpression leads to a >100-fold increase in platelet stores of urokinase plasminogen activator (PLAU/uPA); subsequent plasmin-mediated degradation of diverse α-granule proteins; and platelet-dependent, accelerated fibrinolysis. The causative mutation is a 78-kb tandem duplication of *PLAU*. How this duplication causes megakaryocyte-specific *PLAU* overexpression is unknown. To investigate the mechanism that causes QPD, we used epigenomic profiling, comparative genomics, and chromatin conformation capture approaches to study *PLAU* regulation in cultured megakaryocytes from participants with QPD and unaffected controls. QPD duplication led to ectopic interactions between *PLAU* and a conserved megakaryocyte enhancer found within the same topologically associating domain (TAD). Our results support a unique disease mechanism whereby the reorganization of sub-TAD genome architecture results in a dramatic, cell-type–specific blood disorder phenotype. (*Blood*. 2020;136(23):2679-2690)

Introduction

Quebec platelet disorder (QPD) is an autosomal dominant bleeding disorder with complete penetrance of a unique gain-of-function defect in fibrinolysis.[1] The causative mutation is a 78-kb single-tandem duplication on chromosome 10q22 that includes *PLAU* and its known regulatory elements.[1] *PLAU* is ubiquitously expressed in most nonneuronal solid tissues and shows higher expression in granulocytes and dendritic cells[2] than in megakaryocytes.[3,4] In QPD, a >100-fold increase in *PLAU* expression in megakaryocytes results in platelet-dependent but not systemic fibrinolysis, increasing platelet PLAU/uPA and triggering intraplatelet plasmin generation that degrades diverse α-granule proteins.[4-6] QPD increases risks for challenge-related bleeding (examples in Figure 1A) that can be reduced with antifibrinolytic drugs (the only known effective treatment).[7] Mice that selectively overexpress *PLAU* in megakaryocytes have a QPD-like bleeding disorder.[8]

Discovery of the QPD duplication mutation has transformed diagnostic testing for this blood disorder. However, the molecular mechanism that explains how this mutation causes QPD is unknown. Multiple lines of evidence indicate that QPD results from profound, allele- and megakaryocyte-specific overexpression of *PLAU* by the disease chromosome. First, QPD megakaryocytes and platelets exhibit >100-fold increased levels of structurally normal *PLAU* mRNA[3] and PLAU/uPA protein[4] relative to controls, whereas QPD saliva, urine, monocytes, granulocytes, and CD34$^+$ hematopoietic progenitors show only minimal changes (~2-5-fold).[3-6,9] Second, overexpression of *PLAU* by the disease chromosome emerges with megakaryocyte differentiation, with day-13 to -14 cultured QPD megakaryocytes showing the same >100-fold increase in *PLAU* transcripts and uPA levels in QPD platelets.[6] Third, *PLAU* transcripts overexpressed in QPD megakaryocytes show a strong (>100-fold) bias for alleles from the disease chromosome, unlike those expressed by QPD CD34$^+$ hematopoietic progenitors or granulocytes.[3,5,6]

The 78-kb QPD duplication on chromosome 10q22[1] contains 1 additional gene, *C10orf55*, and is flanked by the neighboring genes *CAMK2G* and *VCL*, located ~37 kb upstream and 87 kb downstream of the *PLAU* promoter, respectively.[1,3] All 4 genes are contained entirely within a ~400-kb topologically associating domain (TAD).[10] TADs are megabase-scale, self-interacting, genomic intervals that can act as evolutionarily conserved regulatory units where enhancers are more likely to access receptive gene promoters.[10-14] Although genes within the same TAD are known to exhibit coordinated patterns of expression,[15,16] TADs can be further partitioned into substructures, such as insulated neighborhoods or

Downloaded from http://ashpublications.net/blood/article-pdf/136/23/2679/1791833/bloodbld2020005394.pdf by guest on 02 June 2024

© 2020 by The American Society of Hematology

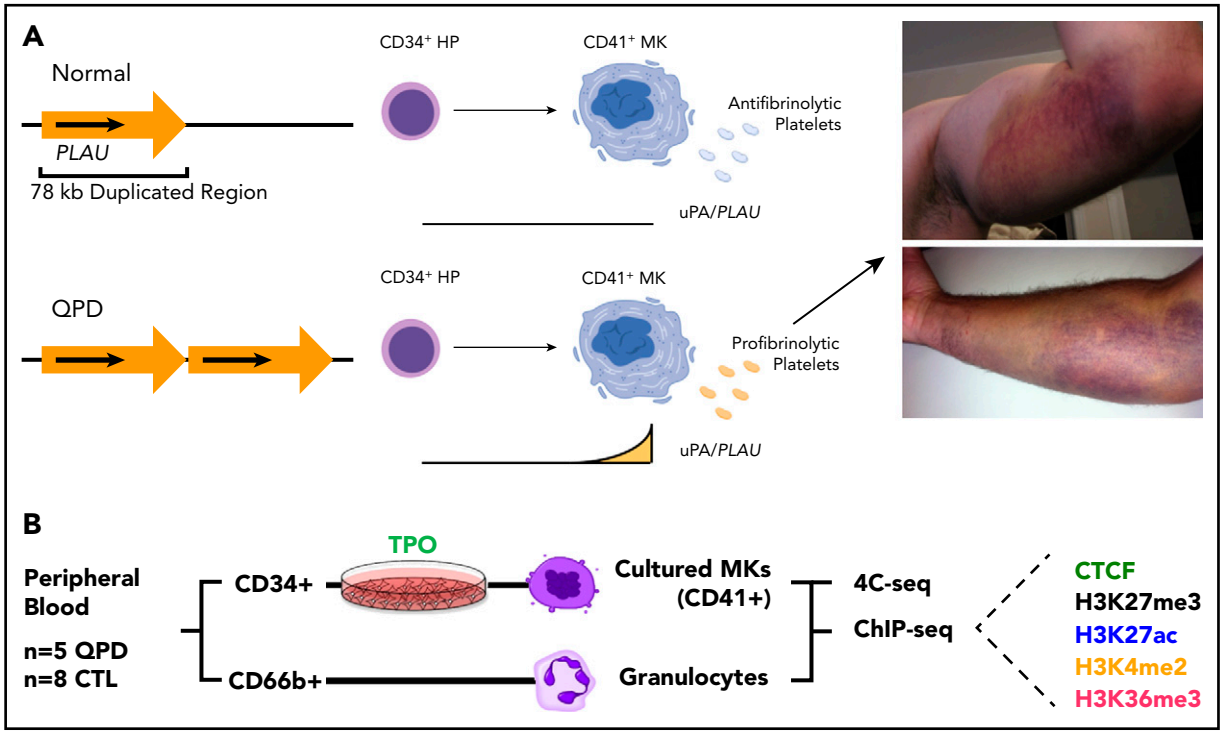

Figure 1. Overview of QPD and study design (A) Overview of QPD pathogenesis. QPD is associated with a duplication mutation of *PLAU* that selectively increases *PLAU* expression with megakaryocyte differentiation, resulting in a platelet-dependent gain-of-function defect in fibrinolysis, with hemostatic consequences. Images show QPD bleeds in 2 participants, after exercise (top) or a minor fall (bottom). (B) Overview of samples, cell types, and experimental assays. TPO, thrombopoietin; MK, megakaryocytes; HP, hematopoietic progenitor. The schematic in panel A was created with BioRender.com.

sub-TADs, that orchestrate spatiotemporal gene expression patterns.[17-23] *PLAU* expression appears to be uncoupled from that of *C10orf55*, *CAMK2G*, and *VCL*. For example, in QPD megakaryocytes, *PLAU* expression is increased >100-fold without affecting that of *C10orf55*, *CAMK2G*, or *VCL*.[3] Similarly, induction of *PLAU* in nonexpressing HepG2 cells results in an ~100-fold increase in *PLAU* expression, with minimal effects on *CAMK2G* and *VCL* expression.[24,25] Furthermore, during normal megakaryocyte differentiation, *PLAU* expression is unchanged, whereas *VCL* expression increases over time.[26] The distinct *PLAU* expression patterns after stimulation and during megakaryopoiesis indicate that sub-TAD structures are integral to this locus.[17-21]

In this study, we asked whether a detailed characterization of the *PLAU* locus, using epigenomic profiling and chromatin conformation capture approaches to compare overexpressing (megakaryocytes) and nonoverexpressing (granulocytes) blood cell types, would reveal the molecular mechanism(s) that gives rise to the QPD phenotype. Our results support a model in which the QPD duplication positions 1 copy of *PLAU* within a neighboring sub-TAD where *PLAU* is ectopically activated by a conserved hematopoietic enhancer during megakaryopoiesis.

Methods

Ethics

Studies were conducted in accordance with the revised Declaration of Helsinki with approval from the Hamilton Integrated Research Ethics Board and the Centre Hospitalier Universitaire Sainte Justine Research Ethics Board. All participants provided written informed consent.

Subjects and sample collection

Peripheral blood samples (≤200 mL per donation) were collected by multiple donations from QPD (n = 5) and age- and sex-matched controls (n = 8; some declined multiple donations). Identities were anonymized at collection and further simplified for publication. Peripheral blood CD66b$^+$ granulocytes and CD34$^+$ hematopoietic progenitors were obtained as described.[6] QPD and control samples were processed in parallel.

Megakaryocyte culture

Megakaryocytes were grown in liquid culture from peripheral blood–derived CD34$^+$ hematopoietic progenitors and assessed for viability and differentiation, as described.[3]

ChIP-seq library preparation and sequencing

Multiple batches of day-14 cultured megakaryocytes and peripheral blood granulocytes were prepared, cross-linked in 1% formaldehyde, and stored at −80°C until use for chromatin immunoprecipitation sequencing (ChIP-seq) and 4C-seq. ChIP libraries were prepared as described.[27] Antibodies included mouse monoclonal anti-H3K27ac (05-1334; Millipore), rabbit polyclonal anti-H3K4me2 (07-030; Millipore), rabbit polyclonal anti-H3K36me3 (ab9050; Abcam), rabbit polyclonal anti-H3K27me3 (07-449; Millipore), and rabbit polyclonal anti-CTCF (07-729; Millipore). All sequencing libraries were constructed using the NEBNext ChIP-seq DNA library preparation kit with the exception of H3K27me3 and CTCF ChIP-seq libraries which used NEBNext Ultra II (cat. no. E7645L). Size selection for 200- to

Downloaded from http://ashpublications.net/blood/article-pdf/136/23/2679/1791833/bloodbld2020005394.pdf by guest on 02 June 2024

350-bp fragments was performed by PippinPrep (Sage Science), quantified with the 2100 Bioanalyzer (Agilent), and sequenced (The Centre for Applied Genomics [TCAG], Toronto, ON, Canada) on a HiSeq2500 for 50-bp single-ended reads.

4C-seq library preparation and sequencing

Primers for 4C-seq were designed using the 4C primer designer (https://mnlab.uchicago.edu/4Cpd/) for the enzyme combination *Dpn*II (primary) and *Nla*III (secondary). Site-specific primers were appended to sequences used for addition of Illumina sequencing adapters by PCR (supplemental Methods; available on the *Blood* Web site). 4C libraries were constructed with frozen, fixed megakaryocytes (all samples processed in parallel) by published methods.[28]

Sanger sequencing of 4C samples

Forward primers were designed against the single-nucleotide polymorphism (SNP)–containing restriction fragments of interest; reverse primers consisted of the 4C reverse primer plus a 5- to 9-bp overhang specific to the ligation product containing the fragment of interest (supplemental Methods). PCR was performed on 4C PCR products, and bands of the expected size were gel purified and submitted for Sanger sequencing (at TCAG), using the forward PCR primer as the sequencing primer.

H3K27me3 ChIP Droplet Digital PCR

Droplet Digital PCR (ddPCR) was performed at TCAG. Detection of rs1916341 was performed on the QX200 Droplet Digital PCR system (Bio-Rad Laboratories, Inc, Hercules, CA) using TaqMan hydrolysis probe chemistry (Thermo Fisher, Waltham, MA) and a predesigned primer and TaqMan probe PLAU_C_11458608_10 (cat. no.; 4351379; Thermo Fisher). QuantaSoft v1.7.4.0917 (Bio-Rad Laboratories) was used to analyze the data. Reference DNA NA19238 (Coriell Institute for Medical Research, Camden, NJ) was included as a heterozygous control. Up to 5 μL of template DNA, corresponding to ~50 ng of ChIP or input library, was used.

ChIP-seq data analysis

Demultiplexed reads were obtained in fastq format (study data sets) or downloaded from the Short Read Archive (published data sets; National Institutes of Health). Reads were trimmed with Trimmomatic[29] to a minimum length of 36 bp and aligned to the hg19 and mm10 reference genome assemblies for human and mouse, respectively, using the Burrows-Wheeler alignment tool with default settings.[30] Reads of low mapping quality ($q > 1$) and reads overlapping ENCODE blacklist regions (https://www.encodeproject.org/annotations/ENCSR636HFF/) were discarded. Individual replicates were assessed for quality, based on ENCODE ChIP-seq guidelines[31] before pooling for peak calling using MACS2 v2.1.2.[32] Peak calling parameters are described in supplemental Methods.

Differential ChIP enrichment analysis

Differential analysis was performed on peaks genome-wide, with DESeq2 v1.24[33] at default settings, using peak-level counts per replicate. Counts from QPD samples were divided by 1.5 to account for the extra copy gain for peaks overlapping the duplicated region (chr10:75659017-75736956). Raw *P*-values (Wald test) were corrected for the number of peaks within the duplicated region to obtain a locus *P*-value (reported in text) using the false discovery rate (FDR). The same approach was used to compare H3K27ac expression between granulocytes and megakaryocytes.

4C-seq data analysis

Demultiplexed reads were obtained in fastq format and filtered for reads beginning with the 4C reading primer sequence, with an edit distance of 1. Domainograms were generated using 4Cseqpipe v0.7[28] for the region (hg19 chr10:75575000-75875000), with the parameters entered as follows: –read_length 70 –stat_type median –trend_resolution 1000.

Zebrafish reporter assays

Zebrafish were maintained and handled per the guidance of the Canadian Council on Animal Care and the Laboratory Animal Services of The Hospital for Sick Children. Embryos were raised at 28.5°C and staged based on morphology. The 375-bp conserved fragment of ENH_{QPD} (hg19 assembly chr10:75716316–75716690; designated as ENH_{QPD_CONS}) was amplified from human genomic DNA (cat. no. G1471; Promega; primers in supplemental Methods).

The ENH_{QPD_CONS} fragment was first cloned into a GFP reporter vector E1b-Tol2-GFP-gateway34 (37846; Addgene), by using the gateway recombination system (cat. no. 11791020; Gateway LR Clonase II Enzyme Mix; Invitrogen). To generate the *Tg*(*ENH*$_{QPD}$*:GFP*)^{hsc96} zebrafish line, we microinjected 25 ng of the E1b-Tol2-GFP-gw plasmid carrying ENH_{QPD_CONS} into wild-type embryos at the 1-cell stage, together with 150 ng Tol2 mRNA, as described.[35] Injected F0 embryos with GFP expression were raised to adulthood and screened for germline transgene carriers. F1 embryos from stable *Tg*(*ENH*$_{QPD\_CONS}$*:GFP*)^{hsc96} carriers were used for RNA in situ hybridization and confocal imaging, as described.[36] In brief, a previously described *gfp* probe[37] was synthesized using a DIG RNA Labeling kit (cat. no. 11277073910; Roche). To generate double-transgenic embryos, a previously described *Tg*(*gata1:DsRed*)^{sd2} line[38] was crossed with the *Tg*(*ENH*$_{QPD\_CONS}$*:GFP*)^{hsc96} fish. Embryos were collected at 24 hours after fertilization (hpf) for confocal imaging.

Luciferase reporter assays

Luciferase activity was measured using the dual-luciferase reporter assay (E1960; Promega), which relies on cotransfection of 2 plasmids: pGL4.23 (firefly luciferase) and pGL4.75 (*Renilla* luciferase). Luciferase activity is calculated by normalizing pGL4.23 firefly signal to pGL4.75 *Renilla* signal. Assayed constructs were generated by subcloning the empty pGL4.23 vector (minP). *PLAU* (p*PLAU*; chr10:75670575-75670944; 315 bp upstream and 55 bp downstream of the transcription start site [TSS])[25] and *VCL* (p*VCL*; chr10:75757517-75757938; 367 bp upstream and 55 bp downstream of the TSS) promoters, and ENH_{QPD_CONS} were PCR amplified from human genomic DNA (cat. no. G1471; Promega). Primers are described in supplemental Methods.

p*PLAU* and p*VCL* were inserted in place of the minimal promoter upstream of the luc2 gene in pGL4.23, using the *Bgl*II and *Nco*I restriction sites. ENH_{QPD_CONS} was inserted downstream of the firefly luciferase gene (luc2), using the *Not*I restriction site. K562 cells were plated at a density of 10^4 cells in 96-well plates with 4 technical replicates for each construct. Separate transfections were performed in 5 plates. The transfections were performed with Lipofectamine 3000 (Thermo Fisher Scientific). For human megakaryocyte transfection, day 5 (donor 1) or day 8 (donor 2) megakaryocytes, at a cell density of 2.5×10^5 cells per well in 6-well plates, were transfected, using Amaxa Human $CD34^+$ Nucleofector Kit according to the manufacturer's protocol. Luciferase activity was

Downloaded from http://ashpublications.net/blood/article-pdf/136/23/2679/1791833/bloodbld2020005394.pdf by guest on 02 June 2024

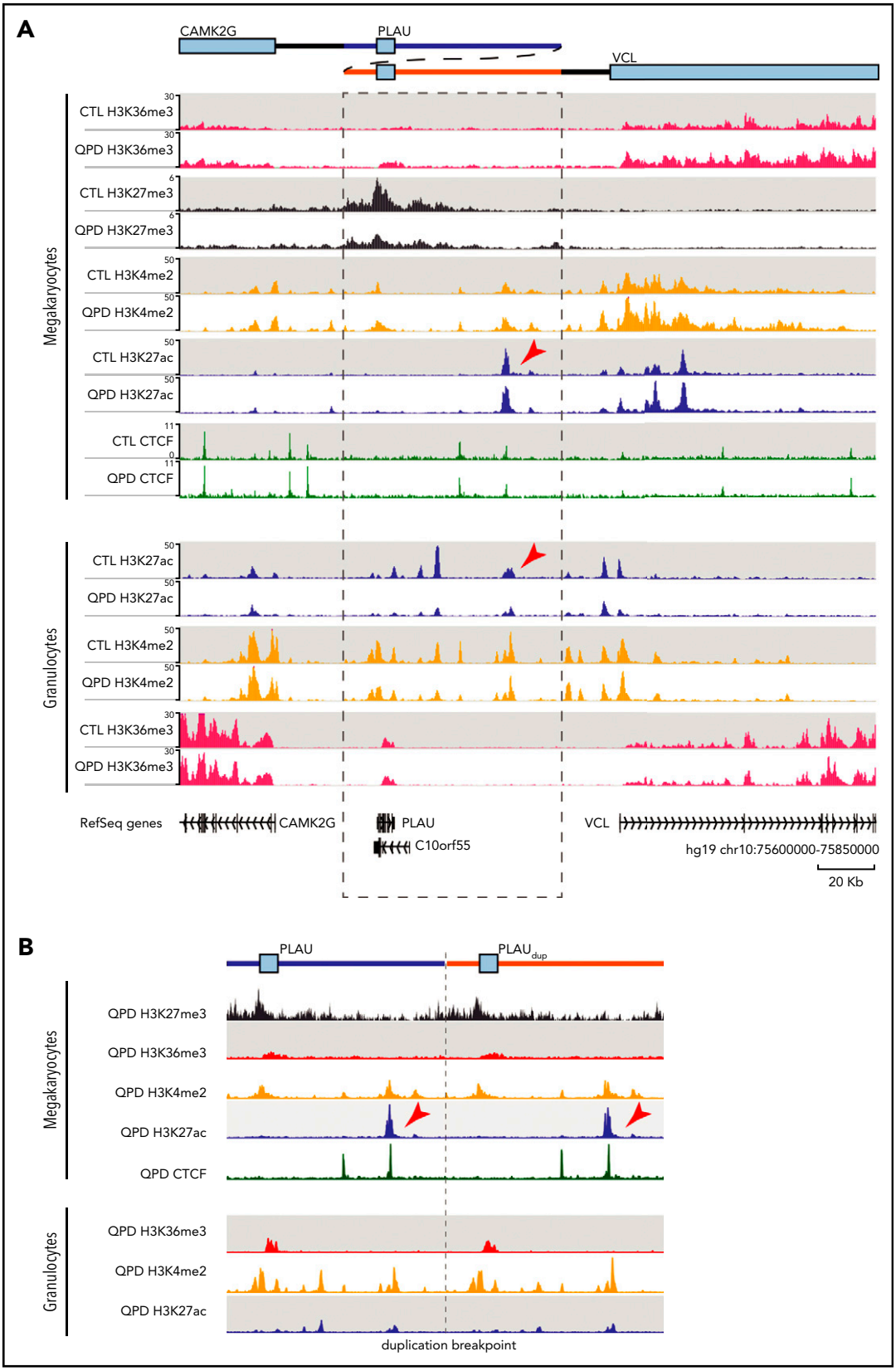

Figure 2. QPD results in a loss of repressive chromatin and repositions *PLAU* relative to a candidate megakaryocyte enhancer. (A) Genome browser view of tracks produced by ChIP-seq of H3K27ac (blue), H3K4me2 (orange), and H3K36me3 (red) in granulocytes and megakaryocytes, from QPD and control (CTL), and H3K27me3 (gray) and CTCF (green) from QPD and CTL megakaryocytes only (bottom). Each track shows merged signal from 3 biological replicates with the exception of the CTL granulocyte H3K4me2, for which only 2 biological replicates were used. ChIP-seq track values are shown as fold change over input. Arrowheads mark the position of ENH_{QPD}. The schematic (top) describes the duplication in QPD. Dashed lines mark the boundaries of the duplicated region. Tracks were visualized using the WashU epigenome browser with the

Downloaded from http://ashpublications.net/blood/article-pdf/136/23/2679/1791833/bloodbld2020005394.pdf by guest on 02 June 2024

measured on the Fluoroskan Ascent FL plate reader. Statistical analysis was performed with 1-way analysis of variance with the Tukey correction.

Results

To understand how the QPD duplication can alter *PLAU* regulation, we obtained CD66b$^+$ granulocytes and CD34$^+$ hematopoietic progenitors from individuals with QPD (n = 5) and control participants (n = 8). CD34$^+$ hematopoietic progenitors were differentiated into megakaryocytes and harvested on day 14 of culture (at harvest: 79%-93% CD41$^+$, with 20-98 ng von Willebrand factor in the medium per 10^6 cells). Cells were subjected to epigenomic profiling by ChIP-seq for the histone posttranslational modifications H3K27ac (mark of active regulatory regions), H3K27me3 (mark of polycomb-mediated repression), H3K4me2 (mark of active and latent enhancers), and H3K36me3 (mark of active transcription). We also profiled CTCF, a zinc finger protein involved in the formation of TAD and sub-TAD boundaries.[19,20,40-42] In addition, we profiled active histone modifications (H3K27ac, H3K4me2, and H3K36me3) in QPD and control peripheral blood granulocytes, a lineage that normally expresses *PLAU*, but does not exhibit allele-specific *PLAU* overexpression in QPD[3] (Figure 1B).

For megakaryocytes, ChIP-seq results indicated a gain in H3K36me3 across the *PLAU* gene body in QPD, which is consistent with an increase in RNA polymerase II (RNAP2)–mediated transcription in QPD megakaryocytes (1.9-fold; FDR = 1.4e−7; Figure 2A). We also observed a reduction in H3K27me3 at the *PLAU* promoter (1.3-fold; FDR = 8e−3) in QPD vs control megakaryocytes (Figure 2A), suggesting that the active expression of *PLAU* in QPD megakaryocytes is associated with a loss of chromatin repression. The remaining factors were highly concordant between control and QPD megakaryocytes within the region duplicated in QPD (QPD duplication; chr10:75659017-75736956; Figure 2A), without significant differences in enrichment for H3K27ac or H3K4me2 peaks within the QPD duplication (FDR < .05). Consistent with our previous work comparing *C10orf55* mRNA and protein expression between QPD megakaryocytes and controls, we did not observe any overt H3K4me2/H3K27ac changes around its TSS, or H3K36me3 enrichment in its gene body (Figure 2A). The breakpoint sequence at the duplication boundaries in QPD samples did not appear to create novel regulatory elements, as no ChIP-seq enrichments were observed when the sequence was aligned with that of an in silico QPD genome that contained the QPD duplication (Figure 2B).

To test whether the loss of H3K27me3 shows bias for the disease chromosome in QPD megakaryocytes, we analyzed the *PLAU* intronic single-nucleotide polymorphism (rs1916341G>T) that falls within the H3K27me3 peak by ddPCR analysis of our H3K27me3 ChIP-seq and matched input libraries from heterozygous individuals with QPD (2 copies of the T allele on the disease chromosome and the G allele on the other). We detected allelic ratios consistent with the expected genomic copy number in all heterozygous input libraries (~2:1 for n = 3 QPD libraries and ~1:1 for n = 1 control library, respectively; supplemental Figure 1). In contrast, the levels of the QPD allele were significantly depleted in H3K27me3 ChIP-seq libraries relative to input for all 3 QPD samples (~1.3:1; $P < 2.2e{-}16$; Fisher's exact test) but not in the control libraries (supplemental Figure 1). This result indicates that the loss of H3K27me3 in QPD megakaryocytes occurs preferentially on the disease chromosome.

To discover enhancers that could drive *PLAU* overexpression in QPD megakaryocytes, we compared H3K27ac enrichment between QPD and control granulocytes and megakaryocytes. We identified 7 H3K27ac peaks within the QPD duplication in QPD and control granulocytes, including the previously studied *PLAU* upstream enhancer[24] (Figure 2A). The only enriched H3K27ac peak in QPD and control megakaryocytes relative to granulocytes (2.9-fold; FDR = 8.0e−6) was a 5.7-kb element that was roughly equidistant (~50 kb) between the *PLAU* and *VCL* promoters (Figure 2A-B; arrowheads). This element ranks within the top 10th percentile of peaks in megakaryocytes when ordered by H3K27ac fold-enrichment, vs >30th percentile in granulocytes (supplemental Figure 2A). Comparing H3K27ac ranking in our samples with cells/tissues from Roadmap Epigenomics,[43] we found that this element was marked by H3K27ac in the majority of hematopoietic cell types profiled, with megakaryocytes ranking among the top cells and tissues[43] (supplemental Figure 2B). Given the H3K27ac enrichment seen in megakaryocytes and other tissues, we designated this putative enhancer as ENH_{QPD}.

Although *PLAU* and *VCL* share conserved synteny and their tandem organization across vertebrates (eg, human and zebrafish), the ENH_{QPD} sequence itself is conserved only in mammals (supplemental Figure 3A). Closer inspection of ENH_{QPD} using published ChIP-seq experiments performed in human megakaryocytes[44] and mouse CD41$^+$ hematopoietic precursors[45] showed conserved orthologous H3K27ac enrichment and binding of canonical megakaryocyte transcription factors, including FLI1, GATA1, RUNX1, and TAL1[46] (Figure 3A-B; supplemental Figure 3B). The conserved *cis* regulatory module (designated ENH_{QPD_CONS}; 91% identity between human and mouse) is a nucleosome-free ~375-bp region that falls in the prominent valley of the conserved H3K27ac signal in both humans and mice.

To ascertain ENH_{QPD} function in vivo, we generated the *Tg*(ENH_{QPD}:*GFP*)^{hsc96} zebrafish reporter line to visualize ENH_{QPD} activity in the developing zebrafish embryo, by using the 375-bp sequence corresponding to ENH_{QPD_CONS} (Figure 3C; supplemental Figure 3B). Despite the absence of a sequence orthologue of ENH_{QPD_CONS} in fish and consistent with conserved regulatory logic and binding preferences of hematopoietic transcription factors, we detected GFP by in situ staining at 24 hpf in tissues that give rise to thrombocytes (the zebrafish equivalent of platelets), among other hematopoietic lineages, later in development[47] (Figure 3D). We validated these expression patterns using a double cross with a gata1:dsRed reporter line, a hematopoietic transcription factor that is tightly restricted to the hematopoietic lineage in fish,[48] and observed colocalization of GFP with dsRed signal (Figure 3E). We concluded that ENH_{QPD} is active in

Figure 2 (continued) following settings: summary method, max; smoothing window, 3 pixels. (B) ChIP-seq signal from QPD megakaryocytes and granulocytes aligned to a custom chromosome 10 containing the QPD duplication. Tracks were smoothed before visualization with Sushi[70] in R. Only unmapped reads and reads mapping to chromosome 10 from hg19 alignments were used.

Downloaded from http://ashpublications.net/blood/article-pdf/136/23/2679/1791833/bloodbld2020005394.pdf by guest on 02 June 2024

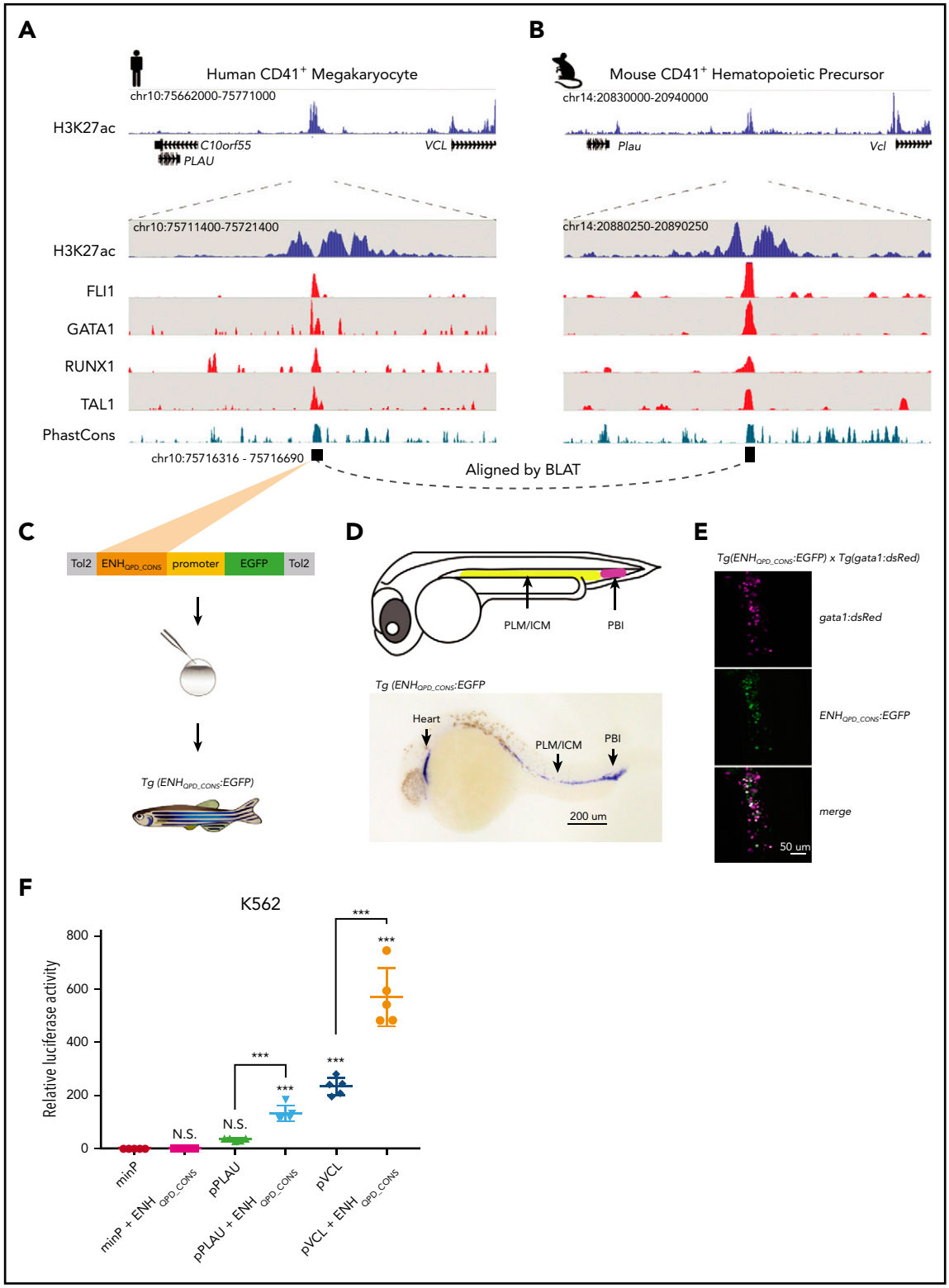

Figure 3. ENH_{QPD} is a conserved hematopoietic enhancer that acts in synergy with the *PLAU* and *VCL* promoters. (A) Views of human ENH_{QPD}. H3K27ac signal from QPD megakaryocytes (blue, including zoom in view) are compared with published ChIP-seq tracks for hematopoietic transcription factors from cord blood–derived megakaryocytes[44] (red), expressed as fold change over input. Teal track shows a 46-way vertebrate PhastCons score. (B) Similar views of the orthologous equivalent of ENH_{QPD} in mouse, showing ChIP-seq tracks for corresponding transcription factors profiled in mouse $CD41^+$ hematopoietic precursor cells.[45] Black squares in panels A and B (bottom) depict ENH_{QPD_CONS}. (C) The Tol2 reporter vector system. (D) An embryo at 24 hpf (top), showing known early-stage zebrafish hematopoietic tissues (adapted from Chen and Zon,[47] with permission); in situ staining (bottom) for GFP in *Tg*(ENH_{QPD_CONS}*:EGFP*). A representative F2 embryo at 24 hpf is shown. Embryos were fixed at 24 hpf in 4% paraformaldehyde and incubated with a digoxigenin-labeled antisense *gfp* probe. RNA-probe hybrids were detected by an alkaline phosphatase–conjugated antibody (anti-digoxigenin-AP and Fab fragments; 1:5000; Roche, Basel, Switzerland) that catalyzed reaction on a chromogenic substrate (NBT/BCIP; Roche). Stained embryos were cleared in 2:1 benzyl benzoate/benzyl alcohol solution and imaged under an Axio Zoom.V16 Stereoscope (Zeiss, Oberkochen, Germany). PLM, posterior lateral mesoderm; ICM, interior cell mass; PBI, posterior blood island.

Downloaded from http://ashpublications.net/blood/article-pdf/136/23/2679/1791833/bloodbld2020005394.pdf by guest on 02 June 2024

zebrafish hematopoietic cells and functions as a conserved hematopoietic enhancer.

During normal megakaryocyte differentiation, *PLAU* expression remains low, whereas *VCL* expression increases considerably (supplemental Figure 4).[26] In QPD megakaryocytes, *PLAU* expression mirrors that of *VCL* and other canonical platelet-expressed genes.[6] Given that the QPD duplication positions a copy of *PLAU* downstream of ENH_{QPD} (Figure 2B), we hypothesized that ENH_{QPD} normally functions as a *VCL* enhancer that is adopted by *PLAU* in QPD.

We next asked whether ENH_{QPD} has the capacity to drive promoter activity, by using a luciferase reporter in human hematopoieticlike cells (K562 cells; which express hematopoietic transcription factors such as *GATA1*, *GATA2*, *NFE2*, and *TAL1*[49]). The addition of ENH_{QPD_CONS} to a minimal promoter (minP) did not elicit enhancer activity in K562 cells (0.90-fold luciferase signal relative to minP; 95% confidence interval, 0.7-1.1; Figure 3F). In contrast, the addition of ENH_{QPD_CONS} to the *PLAU* promoter (p*PLAU*) and *VCL* promoter (p*VCL*) resulted in a 2.4- and 3.7-fold increase in luciferase activity relative to their respective promoter-only equivalents (Figure 3F). This result demonstrates that ENH_{QPD} is promoter specific and can enhance expression of both *PLAU* and *VCL* promoters, which we confirmed with cultured human megakaryocytes (supplemental Figure 5).

We then asked whether DNA topology supports the existence of sub-TAD structure at the *PLAU* locus by interrogating both published in situ Hi-C[10] and CTCF chromatin-interaction analysis by paired-end tag sequencing (ChIA-PET) looping data sets[50] (Figure 4A-B). Inspection of Hi-C contacts in K562 cells revealed that the locus is divided into 2 nested sub-TADs that encompass and separate each of *PLAU* and *VCL*, referred to hereafter as sub-TAD_{PLAU} and sub-TAD_{VCL}, respectively (Figure 4A-B; dashed rectangles). Furthermore, we observed evidence of a strong looping interaction at the boundaries of sub-TAD_{PLAU} in Hi-C contacts from K562 cells, but not in those from IMR90 fibroblasts (Figure 4A; supplemental Figure 6), indicating that sub-TAD boundaries at the *PLAU* locus are tissue specific.

The boundaries of sub-TAD_{PLAU} and sub-TAD_{VCL} coincided with CTCF loop anchors in K562 cells, indicating that these sub-TADs are demarcated by CTCF-CTCF loops. CTCF profiles in K562 cells were representative of our CTCF ChIP-seq from QPD and control megakaryocytes (Figure 4B). This sub-TAD designation also coincided with distinct H3K27ac and H3K27me3 domains in control megakaryocytes, where sub-TAD_{PLAU} was enriched for H3K27me3 and depleted of H3K27ac, whereas sub-TAD_{VCL} was enriched for H3K27ac and depleted of H3K27me3 (Figure 4B). Evaluation of local promoter-enhancer interactions using published human megakaryocyte promoter capture Hi-C data[51] showed that ENH_{QPD} physically interacted with the *VCL* promoter, but not the equidistant *PLAU* promoter, in normal megakaryocytes (Figure 4C). Together, these findings suggest that the *PLAU* locus is partitioned into distinct sub-TADs in normal megakaryocytes as in K562 cells, and that sub-TAD_{PLAU} may function as an "insulated neighborhood,"[17,52] separating *PLAU* from active enhancers in the neighboring sub-TAD_{VCL}.

Because the QPD duplication spans the boundary between sub-TAD_{PLAU} and sub-TAD_{VCL}, such that a copy of *PLAU* is placed ~50 kb downstream of ENH_{QPD} (Figure 4B) and within sub-TAD_{VCL}, we hypothesized that the repositioning of *PLAU* in QPD could enable ectopic enhancer-promoter interactions between ENH_{QPD} and *PLAU*, thereby driving *PLAU* overexpression in QPD megakaryocytes. To determine whether the QPD duplication causes altered enhancer-gene interactions that lead to *PLAU* activation, we interrogated interactions from the *PLAU* promoter and ENH_{QPD} perspectives by performing 4C-seq[39] in QPD and control megakaryocytes. In control megakaryocytes, interactions from the *PLAU* promoter perspective are mostly confined within sub-TAD_{PLAU}. By contrast, interactions from the ENH_{QPD} perspective are enriched at multiple positions coinciding with H3K27ac peaks within sub-TAD_{VCL}, including the *VCL* promoter, but are depleted at equidistant regions beyond the boundary between sub-TAD_{PLAU} and sub-TAD_{VCL} (Figure 5A-B). These indicate that the sub-TAD boundary physically separates *PLAU* from ENH_{QPD} and other active elements in normal megakaryocytes. In QPD megakaryocytes, *PLAU* promoter interactions crossed the sub-TAD boundary and were enriched within the section of the QPD duplication that falls within sub-TAD_{VCL} and includes ENH_{QPD}. Similarly, ENH_{QPD} interactions crossed the sub-TAD boundary and were enriched within the duplicated region upstream of *PLAU*, together indicating the occurrence of ectopic interactions between *PLAU* and ENH_{QPD} (Figure 5B).

Given these 4C-seq results, we asked if interactions between ENH_{QPD} and *PLAU* in QPD megakaryocytes show a concordant bias for the disease chromosome. Genotyping results identified 2 independent *PLAU* SNPs in 4 QPD participants: rs1916341G>T and rs2227574delG (found on 2 distinct *Dpn*II fragments; locations shown in Figure 5D). Allele-specific analysis of 4C-seq reads from the ENH_{QPD} perspective revealed bias in the percentage of reads containing the QPD allele for rs2227574 (expected, 66.6%; median, 92.3%; range observed, 82.0% to 100%) and for rs1916341 (expected, 66.6%; median, 88.0%; range observed, 61.9% to 95.2%) (Figure 5D). Sanger sequencing on 4C libraries for 1 control sample (C8) that was heterozygous at rs1916341 supports that both alleles were detected at similar levels in control megakaryocytes (Figure 5E). Together, our findings indicate that QPD results in allele-specific ectopic interactions between *PLAU* and ENH_{QPD}, suggesting that sub-TAD organization is disrupted on the disease chromosome.

Figure 3 (continued) (E) Confocal microscopy image of the PBI in a representative *Tg(gata1:dsRed)* x *Tg(ENH$_{QPD_CONS}$:EGFP)* double-transgenic embryo. At 24 hpf, embryos were mounted in 1% (w/v) low-melt agarose (Sigma-Aldrich, St. Louis, MO) and imaged under a Nikon A1R Si Point scanning confocal microscope (Nikon, Tokyo, Japan). (F) Relative luciferase activity for minimal (minP), *PLAU* (pPLAU), or *VCL* (pVCL) promoter constructs, with or without ENH_{QPD_CONS}, assayed in K562 erythroid leukemia cells. Data points show measured values averaged from 4 technical replicates (separate wells) per construct, for 5 separate transfections. All values were normalized relative to minP in their respective cell type. Statistical analysis was performed using 1-way analysis of variance with the Tukey correction. Asterisks immediately above data points denote significance compared with minP. Error bars show standard deviation of mean. Asterisks denote significance vs minP and other select pairwise comparisons. ***$P < .001$; n.s., not significant. All constructs and inserted sequences are further described in "Materials and methods" and supplemental Methods.

Downloaded from http://ashpublications.net/blood/article-pdf/136/23/2679/1791833/bloodbld2020005394.pdf by guest on 02 June 2024

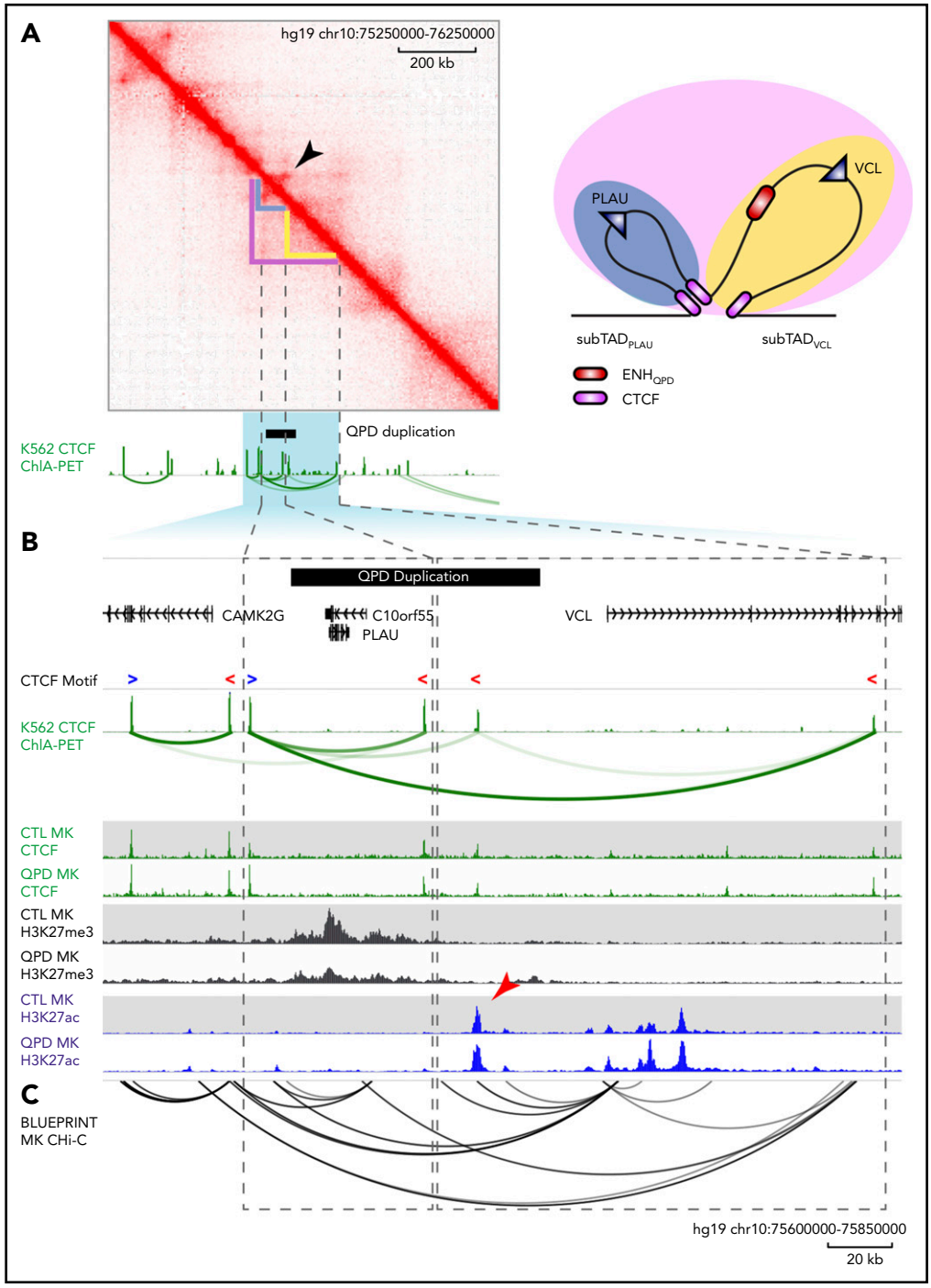

Figure 4. The QPD duplication spans the sub-TAD boundary separating *PLAU* and ENH$_{QPD}$. (A) Hi-C interaction matrix from K562 erythroid leukemia cells. Green tracks show K562 CTCF ChIP-seq and ChIA-PET interactions. Arrowhead marks a corner-dot feature, indicative of a looping interaction. A graphic interpretation (right) of the sub-TAD structures. Domains are color coded corresponding to structures marked on the Hi-C interaction matrix: blue, sub-TAD$_{PLAU}$; yellow, sub-TAD$_{VCL}$. CTCF sites are shown in purple. (B) Zoom-in of the highlighted region in panel A. K562 CTCF ChIP-seq ChIA-PET interactions (top) as in panel A. Blue ">" and red "<" depict forward- and reverse-oriented CTCF motifs, respectively. H3K27ac (blue) and H3K27me3 (gray) and CTCF (green) ChIP-seq tracks (bottom) from QPD and control megakaryocytes (MK), as in Figure 2. Black bar marks the region duplicated in QPD. Dashed rectangles mark the inferred inactive sub-TAD$_{PLAU}$ (left) and active sub-TAD$_{VCL}$ (right) domains. Arrowhead marks the position of ENH$_{QPD}$. (C) Black arcs show the megakaryocyte promoter capture Hi-C interactions reported by Javierre et al.[51] Only interactions with a soft-thresholded, negative log-weighted $P \geq 5$ are shown.

Discussion

The question of how a single tandem duplication results in a profound cell-type–specific overexpression of the clot-breaking enzyme PLAU in QPD has been a long-standing mystery. In this study, QPD duplication positioned a copy of *PLAU* within a neighboring sub-TAD, placing it under the control of a conserved megakaryocyte enhancer (Figure 6). Given the association of H3K27me3 with the native *PLAU* promoter in normal megakaryocytes, and the loss of H3K27me3 specific to the disease

Downloaded from http://ashpublications.net/blood/article-pdf/136/23/2679/1791833/bloodbld2020005394.pdf by guest on 02 June 2024

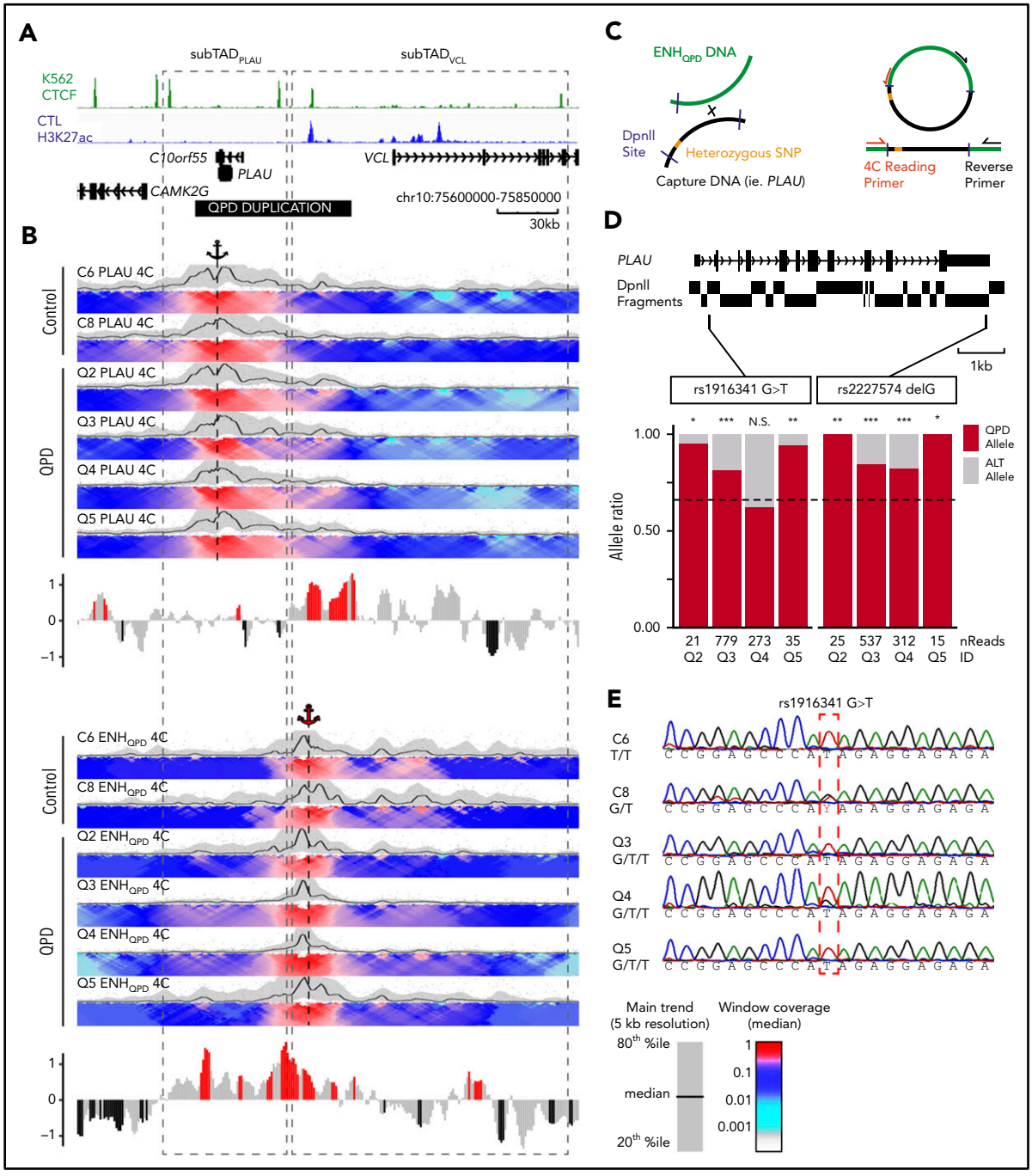

Figure 5. QPD results in ectopic enhancer-gene interactions specific to the disease chromosome. (A) H3K27ac tracks from control megakaryocytes, CTCF ChIA-PET tracks from K562, and gray-dashed boxes marking sub-TAD$_{PLAU}$ and sub-TAD$_{VCL}$ are shown, as in Figure 4. Black horizontal bar marks the position of the QPD duplication. (B) Individual 4C-Seq contact profiles from QPD and control megakaryocytes generated using a bait (restriction fragment) at the *PLAU* promoter (top) and EHN$_{QPD}$ (bottom), marked by black and red anchor symbols, respectively. For domainograms, the black trendline shows the median contact frequency in 5-kb windows tiled across 1-kb increments normalized to the maximum median value at 5-kb resolution; shaded area indicates the 20th to 80th percentiles. The heat map color-scale shows median contact frequency in the windows of increasing size from 2 to 50 kb tiled across 1-kb increments, normalized relative to the maximum median value at 12-kb resolution. Bar plots below domainograms depict log2 fold enrichment in 4C contacts in QPD vs control samples calculated for 5-kb bins tiled across 1-kb increments. Counts for bins falling within the duplicated region were divided by 1.5 to adjust for the copy number in the QPD samples. Red and black bars signify windows of nominally significantly increased interaction in QPD and control samples, respectively (nonadjusted $P < .1$; 2-tailed Student *t* test). (C) The 4C-seq design used to assess allele-specific contacts from the ENH$_{QPD}$ perspective. (D) Genome browser view (top) of *PLAU DpnII* fragments (black rectangles below the gene model) and SNPs rs1916341 and rs2227574 (vertical black bars). Fragments harboring SNPs are outlined in red. The percentage of reads (bottom) from each 4C sample at 2 SNPs that contain either the allele from the disease chromosome or the other allele. Dashed black line show the expected frequency of QPD alleles based on 1.5 copy (ie, 0.66). Numbers below bars correspond to the total number of reads mapped to a given SNP. (E) Sanger sequencing chromatographs of 4C prelibrary PCR products from 2 control and 3 QPD samples. Genotypes are displayed in the format control allele > QPD allele. $*P < .01$; $**P < .001$; $***P < .0001$ by 2-tailed binomial test.

Downloaded from http://ashpublications.net/blood/article-pdf/136/23/2679/1791833/bloodbld2020005394.pdf by guest on 02 June 2024

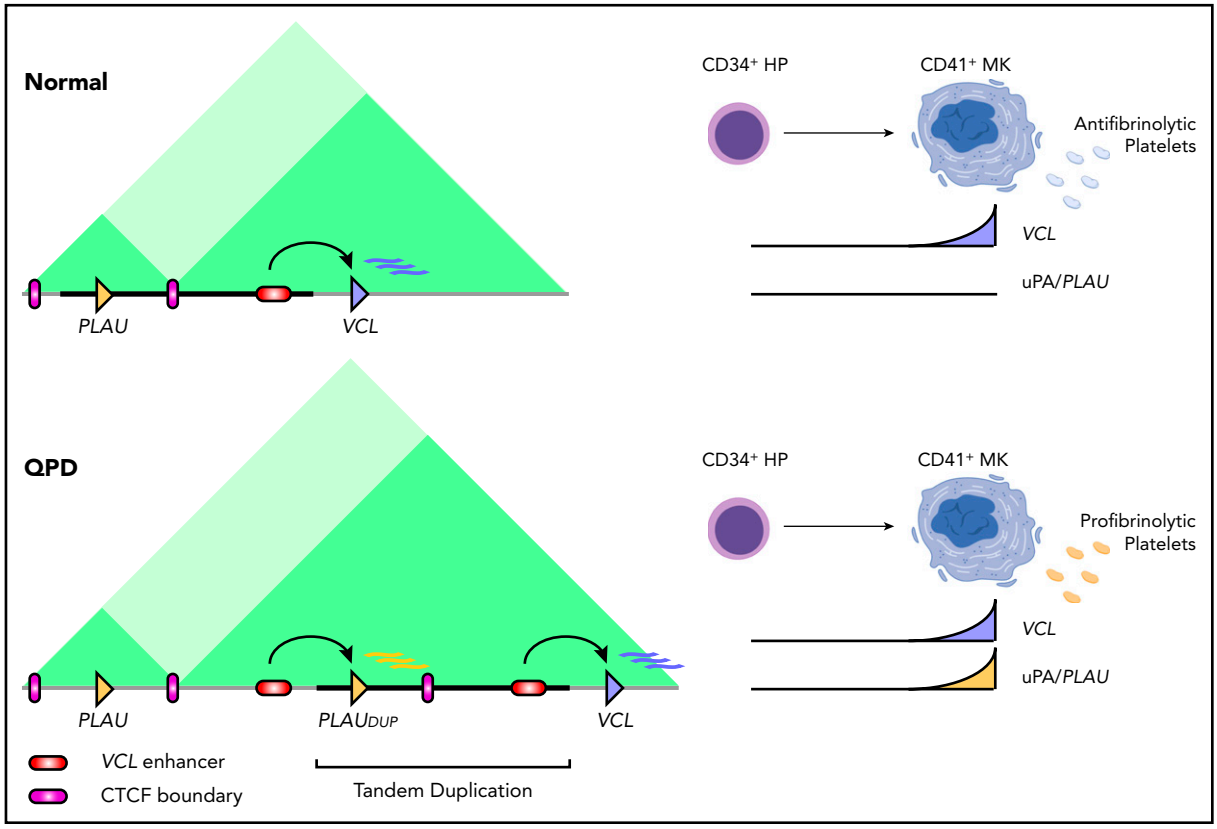

Figure 6. Model of enhancer adoption in QPD. Regulatory interactions at the PLAU locus in megakaryocytes for control (top) vs the QPD (bottom) chromosome. Dark green rectangles mark sub-TAD$_{PLAU}$ and sub-TAD$_{VCL}$. Bold black line marks the QPD duplication. HP, hematopoietic progenitor; MK, megakaryocyte.

chromosome in QPD (supplemental Figure 2), we also propose that the magnitude of *PLAU* expression in QPD stems from a loss of epigenetic silencing at a strong *PLAU* promoter that is triggered via activation by ENH$_{QPD}$ during megakaryopoiesis. The mechanism offers an explanation for the >100-fold increased uPA in QPD platelets that increase risks for experiencing challenge-related bleeding, heavy menstrual bleeding, joint bleeds, spontaneous hematuria (in those with the highest platelet uPA levels), and wound-healing problems that respond to antifibrinolytic therapy.[7,53]

Although several lines of evidence support our model, including experiments using primary cells for individuals with QPD, further mechanistic insight could be gained from future experiments that attempt to reconstruct a minimal QPD duplication through the insertion of ENH$_{QPD}$ within the existing *PLAU* sub-TAD domain. Such an experiment could clarify the contribution of ENH$_{QPD}$ from the larger sub-TAD rearrangement in QPD which includes additional genomic elements: for example, duplication of the conserved CTCF binding sites at the downstream boundary of sub-TAD$_{PLAU}$ that have been demonstrated to be involved in long-range chromatin interactions.

An increasing number of human congenital disorders and cancers have been shown to involve disruptions in 3-dimensional (3D) genome architecture that give rise to ectopic enhancer-gene interactions and consequent pathological changes in gene expression.[54-62] Disruptions in TAD architecture explain the mechanistic basis of many seminal leukemogenic structural mutations that bring transcriptional enhancers in proximity to proto-oncogenes (reviewed in Bhagwat et al[63] and Bresnick and Johnson[64]), such as the t(8;14) translocation involving the *IgH* 3′ enhancer and *MYC* in Burkitt lymphoma,[65] the t(4;14) translocation involving *IgH* enhancers and *MMSET* in multiple myeloma,[66] and the 3q21;q26 inversion involving *GATA2* h-77 enhancer and *MECOM* in AML.[67,68] Together, these diseases, referred to as "enhanceropathies" or "tadopathies,"[69] highlight enhancer dysfunction resulting from disrupted 3D genome architecture as an emerging cause of human disease.

The majority of enhanceropathies/tadopathies reported thus far describe megabase- or chromosome-scale rearrangements that span the boundaries of megabase-scale TADs.[54,56,57] Through fine-mapping of enhancers, CTCF boundary elements, and 3D chromatin architecture in a disease-relevant cell type, we demonstrated that QPD is a unique bleeding disorder enhanceropathy/tadopathy arising from disruption of a single-gene sub-TAD. We predict that other mutations that either disrupt local sub-TAD architecture or juxtapose *PLAU* and ENH$_{QPD}$ in the absence of an intervening boundary element could similarly cause a QPD-like defect. Our findings demonstrate how rewiring of structural elements within TADs can impact evolutionarily conserved cell-type–specific regulatory logic to result in human disease and underscores the importance of considering sub-TAD DNA topology when studying structural genomic variations such as inversions, duplications, and deletions.[54,56]

Acknowledgments

The authors thank the persons with QPD and volunteers who served as controls for participating in the study; The Centre for Applied Genomics

Downloaded from http://ashpublications.net/blood/article-pdf/136/23/2679/1791833/bloodbld2020005394.pdf by guest on 02 June 2024

(TCAG) for assistance with next-generation sequencing; Bing Ren for training in the 4C-seq method and analysis; and Alejandra Medina-Rivera, Mathieu Lupien, and Lincoln Stein for helpful advice regarding experiments and analysis.

Funding for this project was provided by Canadian Institutes of Health Research (CIHR) grant 201603PJT-364832 (C.P.M.H., J.A.M., M.D.W.); an Early Researcher Award from the Ontario Ministry of Research and Innovation and Tier 2 Canada Research Chairs from CIHR (M.D.W.); a Sickkids Restracomp Fellowship (M.L.); the Natural Sciences and Engineering Research Council of Canada-Canada Graduate Scholarships-Master's Program (NSERC-CGS-M) (L.A.); and a Youth Abroad Scholarship from the Ministry of Education of Azerbaijan (A.A.). This study made use of data generated by the Blueprint Consortium. A full list of the investigators who contributed to the generation of the data is available from http://www.blueprint-epigenome.eu. Funding for Blueprint was provided by the European Union's Seventh Framework Programme (FP7/2007-2013) under Grant Agreement 282510-Blueprint.

Authorship

Contribution: M.L. performed bioinformatic analyses and 4C experiments and led the writing of the manuscript; A.S., L.A., L.U.-R., S.A.A., and S.T. performed ChIP-seq experiments; A.A., S.T., L.E.A., and J.A.M. performed and designed the luciferase assays. A.S. and S.T. obtained control samples and performed megakaryocyte cell cultures, genotyping, and qPCR experiments; X.Y. and I.C.S. designed and performed zebrafish experiments; C.P.M.H. and G.-É.R. obtained QPD samples; A.D.P., C.P.M.H., J.A.M., and M.D.W. were involved in conceptualization, supervision, funding acquisition, data interpretation, and experimental design; and all authors edited and approved the manuscript.

Conflict-of-interest disclosure: The authors declare no competing financial interests.

ORCID profiles: M.L., 0000-0002-4451-0921; S.T., 0000-0002-8859-4119; L.E.A., 0000-0003-1051-7997; A.A., 0000-0002-2313-965X; X.Y., 0000-0001-5193-9964; L.A., 0000-0002-8307-3306; S.A.A., 0000-0003-4308-8244; A.D.P., 0000-0002-9169-118X; I.C.S., 0000-0001-6665-1410; J.A.M., 0000-0002-7147-4604; C.P.M.H., 0000-0002-2843-0817; M.D.W., 0000-0002-4015-3066.

Correspondence: Catherine P. M. Hayward, Department of Pathology and Molecular Medicine, McMaster University, Hamilton, ON L8N 3Z5, Canada; e-mail: haywrdc@mcmaster.ca; and Michael D. Wilson, SickKids Research Institute, 686 Bay St, Room 14.9712, Toronto, ON M5G 0A4, Canada; e-mail: michael.wilson@sickkids.ca.

Footnotes

Submitted 28 April 2020; accepted 6 July 2020; prepublished online on *Blood* First Edition 14 July 2020. DOI 10.1182/blood.2020005394.

*C.P.M.H. and M.D.W. contributed equally to this study.

The raw sequencing data sets have been deposited in the European Genotype-phenome Archive (accession number EGAS00001004315) with controlled-access administered by C.P.M.H., as stipulated by participants' consent forms.

All count-level QPD and control ChIP-seq data sets can be downloaded and inspected from the following WashU epigenome browser session site: http://epigenomegateway.wustl.edu/legacy/?genome=hg19&session=rGXGCUCEpa&statusId=423397932. The 4C-seq count data in the format generated by 4Cseqpipe are available in the online data supplement; all previously published data sets used in this publication are listed in the supplemental Methods. Further information and requests regarding data and data analysis should be directed to the corresponding authors: C.P.M.H. (haywrdc@mcmaster.ca) and M.D.W. (michael.wilson@sickkids.ca).

The online version of this article contains a data supplement.

There is a *Blood* Commentary on this article in this issue.

The publication costs of this article were defrayed in part by page charge payment. Therefore, and solely to indicate this fact, this article is hereby marked "advertisement" in accordance with 18 USC section 1734.

Downloaded from http://ashpublications.net/blood/article-pdf/136/23/2679/1791833/bloodbld2020005394.pdf by guest on 02 June 2024

REFERENCES

1. Paterson AD, Rommens JM, Bharaj B, et al. Persons with Quebec platelet disorder have a tandem duplication of PLAU, the urokinase plasminogen activator gene. *Blood*. 2010; 115(6):1264-1266.
2. Uhlén M, Fagerberg L, Hallström BM, et al. Proteomics. Tissue-based map of the human proteome. *Science*. 2015;347(6220):1260419.
3. Hayward CPM, Liang M, Tasneem S, et al. The duplication mutation of Quebec platelet disorder dysregulates PLAU, but not C10orf55, selectively increasing production of normal PLAU transcripts by megakaryocytes but not granulocytes. *PLoS One*. 2017;12(3): e0173991.
4. Kahr WH, Zheng S, Sheth PM, et al. Platelets from patients with the Quebec platelet disorder contain and secrete abnormal amounts of urokinase-type plasminogen activator. *Blood*. 2001;98(2):257-265.
5. Diamandis M, Paterson AD, Rommens JM, et al. Quebec platelet disorder is linked to the urokinase plasminogen activator gene (PLAU) and increases expression of the linked allele in megakaryocytes. *Blood*. 2009;113(7): 1543-1546.
6. Veljkovic DK, Rivard GE, Diamandis M, Blavignac J, Cramer-Bordé EM, Hayward CP. Increased expression of urokinase plasminogen activator in Quebec platelet disorder is linked to megakaryocyte differentiation. *Blood*. 2009;113(7):1535-1542.
7. McKay H, Derome F, Haq MA, et al. Bleeding risks associated with inheritance of the Quebec platelet disorder. *Blood*. 2004;104(1):159-165.
8. Kufrin D, Eslin DE, Bdeir K, et al. Antithrombotic thrombocytes: ectopic expression of urokinase-type plasminogen activator in platelets. *Blood*. 2003;102(3):926-933.
9. Diamandis M, Veljkovic DK, Derome F, Rivard GE, Hayward CP. Evaluation of urokinase plasminogen activator in urine from individuals with Quebec platelet disorder. *Blood Coagul Fibrinolysis*. 2008;19(5):463-464.
10. Rao SSP, Huntley MH, Durand NC, et al. A 3D map of the human genome at kilobase resolution reveals principles of chromatin looping [published correction appears in *Cell*. 2015; 162(3):687-688]. *Cell*. 2014;159(7):1665-1680.
11. Dixon JR, Selvaraj S, Yue F, et al. Topological domains in mammalian genomes identified by analysis of chromatin interactions. *Nature*. 2012;485(7398):376-380.
12. Sexton T, Yaffe E, Kenigsberg E, et al. Three-dimensional folding and functional organization principles of the Drosophila genome. *Cell*. 2012;148(3):458-472.
13. Sexton T, Cavalli G. The role of chromosome domains in shaping the functional genome. *Cell*. 2015;160(6):1049-1059.
14. Jin F, Li Y, Dixon JR, et al. A high-resolution map of the three-dimensional chromatin interactome in human cells. *Nature*. 2013; 503(7475):290-294.
15. Le Dily F, Baù D, Pohl A, et al. Distinct structural transitions of chromatin topological domains correlate with coordinated hormone-induced gene regulation. *Genes Dev*. 2014; 28(19):2151-2162.
16. Nora EP, Lajoie BR, Schulz EG, et al. Spatial partitioning of the regulatory landscape of the X-inactivation centre. *Nature*. 2012;485(7398): 381-385.
17. Dowen JM, Fan ZP, Hnisz D, et al. Control of cell identity genes occurs in insulated neighborhoods in mammalian chromosomes. *Cell*. 2014;159(2):374-387.
18. Smith EM, Lajoie BR, Jain G, Dekker J. Invariant TAD Boundaries Constrain Cell-Type-Specific Looping Interactions between Promoters and Distal Elements around the CFTR Locus. *Am J Hum Genet*. 2016;98(1): 185-201.
19. Narendra V, Bulajić M, Dekker J, Mazzoni EO, Reinberg D. CTCF-mediated topological boundaries during development foster appropriate gene regulation. *Genes Dev*. 2016; 30(24):2657-2662.
20. Hanssen LLP, Kassouf MT, Oudelaar AM, et al. Tissue-specific CTCF-cohesin-mediated

chromatin architecture delimits enhancer interactions and function in vivo. *Nat Cell Biol*. 2017;19(8):952-961.

21. Phillips-Cremins JE, Sauria MEG, Sanyal A, et al. Architectural protein subclasses shape 3D organization of genomes during lineage commitment. *Cell*. 2013;153(6):1281-1295.

22. Hnisz D, Day DS, Young RA. Insulated neighborhoods: structural and functional units of mammalian gene control. *Cell*. 2016;167(5):1188-1200.

23. Sun F, Chronis C, Kronenberg M, et al. Promoter-Enhancer Communication Occurs Primarily within Insulated Neighborhoods. *Mol Cell*. 2019;73(2):250-263.e5.

24. Ferrai C, Munari D, Luraghi P, et al. A transcription-dependent micrococcal nuclease-resistant fragment of the urokinase-type plasminogen activator promoter interacts with the enhancer. *J Biol Chem*. 2007;282(17):12537-12546.

25. Ferrai C, Xie SQ, Luraghi P, et al. Poised transcription factories prime silent uPA gene prior to activation. *PLoS Biol*. 2010;8(1):e1000270.

26. Shim M-H, Hoover A, Blake N, Drachman JG, Reems JA. Gene expression profile of primary human CD34+CD38lo cells differentiating along the megakaryocyte lineage. *Exp Hematol*. 2004;32(7):638-648.

27. Schmidt D, Wilson MD, Spyrou C, Brown GD, Hadfield J, Odom DT. ChIP-seq: using high-throughput sequencing to discover protein-DNA interactions. *Methods*. 2009;48(3):240-248.

28. van de Werken HJG, Landan G, Holwerda SJB, et al. Robust 4C-seq data analysis to screen for regulatory DNA interactions. *Nat Methods*. 2012;9(10):969-972.

29. Bolger AM, Lohse Mdel B. Trimmomatic: a flexible trimmer for Illumina sequence data. *Bioinformatics*. 2014;30(15):2114-2120.

30. Li H, Durbin R. Fast and accurate short read alignment with Burrows-Wheeler transform. *Bioinformatics*. 2009;25(14):1754-1760.

31. Landt SG, Marinov GK, Kundaje A, et al. ChIP-seq guidelines and practices of the ENCODE and modENCODE consortia. *Genome Res*. 2012;22(9):1813-1831.

32. Zhang Y, Liu T, Meyer CA, et al. Model-based analysis of ChIP-Seq (MACS). *Genome Biol*. 2008;9(9):R137.

33. Love MI, Huber W, Anders S. Moderated estimation of fold change and dispersion for RNA-seq data with DESeq2. *Genome Biol*. 2014;15(12):550.

34. Li Q, Ritter D, Yang N, et al. A systematic approach to identify functional motifs within vertebrate developmental enhancers. *Dev Biol*. 2010;337(2):484-495.

35. Kawakami K. Transposon tools and methods in zebrafish. *Dev Dyn*. 2005;234(2):244-254.

36. Thisse C, Thisse B. High-resolution in situ hybridization to whole-mount zebrafish embryos. *Nat Protoc*. 2008;3(1):59-69.

37. Yuan X, Song M, Devine P, Bruneau BG, Scott IC, Wilson MD. Heart enhancers with deeply conserved regulatory activity are established early in zebrafish development. *Nat Commun*. 2018;9(1):4977.

38. Traver D, Paw BH, Poss KD, Penberthy WT, Lin S, Zon LI. Transplantation and in vivo imaging of multilineage engraftment in zebrafish bloodless mutants. *Nat Immunol*. 2003;4(12):1238-1246.

39. van de Werken HJG, de Vree PJP, Splinter E, et al. 4C technology: protocols and data analysis. *Methods Enzymol*. 2012;513:89-112.

40. Kentepozidou E, Aitken SJ, Feig C, et al. Clustered CTCF binding is an evolutionary mechanism to maintain topologically associating domains. *Genome Biol*. 2020;21(1):5.

41. Tang Z, Luo OJ, Li X, et al. CTCF-Mediated Human 3D Genome Architecture Reveals Chromatin Topology for Transcription. *Cell*. 2015;163(7):1611-1627.

42. Vietri Rudan M, Barrington C, Henderson S, et al. Comparative Hi-C reveals that CTCF underlies evolution of chromosomal domain architecture. *Cell Rep*. 2015;10(8):1297-1309.

43. Kundaje A, Meuleman W, Ernst J, et al; Roadmap Epigenomics Consortium. Integrative analysis of 111 reference human epigenomes. *Nature*. 2015;518(7539):317-330.

44. Tijssen MR, Cvejic A, Joshi A, et al. Genome-wide analysis of simultaneous GATA1/2, RUNX1, FLI1, and SCL binding in megakaryocytes identifies hematopoietic regulators. *Dev Cell*. 2011;20(5):597-609.

45. Goode DK, Obier N, Vijayabaskar MS, et al. Dynamic gene regulatory networks drive hematopoietic specification and differentiation. *Dev Cell*. 2016;36(5):572-587.

46. Tijssen MR, Ghevaert C. Transcription factors in late megakaryopoiesis and related platelet disorders. *J Thromb Haemost*. 2013;11(4):593-604.

47. Chen AT, Zon LI. Zebrafish blood stem cells. *J Cell Biochem*. 2009;108(1):35-42.

48. Meng A, Tang H, Yuan B, Ong BA, Long Q, Lin S. Positive and negative cis-acting elements are required for hematopoietic expression of zebrafish GATA-1. *Blood*. 1999;93(2):500-508.

49. Wang H, Hu H, Zhang Q, et al. Dynamic transcriptomes of human myeloid leukemia cells. *Genomics*. 2013;102(4):250-256.

50. Davis CA, Hitz BC, Sloan CA, et al. The Encyclopedia of DNA elements (ENCODE): data portal update. *Nucleic Acids Res*. 2018;46(D1):D794-D801.

51. Javierre BM, Burren OS, Wilder SP, et al; BLUEPRINT Consortium. Lineage-Specific Genome Architecture Links Enhancers and Non-coding Disease Variants to Target Gene Promoters. *Cell*. 2016;167(5):1369-1384.e19.

52. Oti M, Falck J, Huynen MA, Zhou H. CTCF-mediated chromatin loops enclose inducible gene regulatory domains. *BMC Genomics*. 2016;17(1):252.

53. Hayward CPM, Tasneem S, Rivard GE. Thrombopoietin levels in Quebec platelet disorder-Implications for the mechanism of thrombocytopenia. *Int J Lab Hematol*. 2018;40(2):e33-e34.

54. Lupiáñez DG, Kraft K, Heinrich V, et al. Disruptions of topological chromatin domains cause pathogenic rewiring of gene-enhancer interactions. *Cell*. 2015;161(5):1012-1025.

55. Hnisz D, Weintraub AS, Day DS, et al. Activation of proto-oncogenes by disruption of chromosome neighborhoods. *Science*. 2016;351(6280):1454-1458.

56. Franke M, Ibrahim DM, Andrey G, et al. Formation of new chromatin domains determines pathogenicity of genomic duplications. *Nature*. 2016;538(7624):265-269.

57. Kaiser VB, Semple CA. When TADs go bad: chromatin structure and nuclear organisation in human disease [version 1; peer review: 2 approved]. *F1000 Res*. 2017;6:F1000 Faculty Rev-314.

58. Flöttmann R, Kragesteen BK, Geuer S, et al. Noncoding copy-number variations are associated with congenital limb malformation. *Genet Med*. 2018;20(6):599-607.

59. Weischenfeldt J, Dubash T, Drainas AP, et al. Pan-cancer analysis of somatic copy-number alterations implicates IRS4 and IGF2 in enhancer hijacking. *Nat Genet*. 2017;49(1):65-74.

60. Beroukhim R, Zhang X, Meyerson M. Copy number alterations unmasked as enhancer hijackers. *Nat Genet*. 2016;49(1):5-6.

61. Taberlay PC, Achinger-Kawecka J, Lun ATL, et al. Three-dimensional disorganization of the cancer genome occurs coincident with long-range genetic and epigenetic alterations. *Genome Res*. 2016;26(6):719-731.

62. Wu P, Li T, Li R, et al. 3D genome of multiple myeloma reveals spatial genome disorganization associated with copy number variations. *Nat Commun*. 2017;8(1):1937.

63. Bhagwat AS, Lu B, Vakoc CR. Enhancer dysfunction in leukemia. *Blood*. 2018;131(16):1795-1804.

64. Bresnick EH, Johnson KD. Blood disease-causing and -suppressing transcriptional enhancers: general principles and *GATA2* mechanisms. *Blood Adv*. 2019;3(13):2045-2056.

65. Battey J, Moulding C, Taub R, et al. The human c-myc oncogene: structural consequences of translocation into the IgH locus in Burkitt lymphoma. *Cell*. 1983;34(3):779-787.

66. Chesi M, Nardini E, Lim RSC, Smith KD, Kuehl WM, Bergsagel PL. The t(4;14) translocation in myeloma dysregulates both FGFR3 and a novel gene, MMSET, resulting in IgH/MMSET hybrid transcripts. *Blood*. 1998;92(9):3025-3034.

67. Yamazaki H, Suzuki M, Otsuki A, et al. A remote GATA2 hematopoietic enhancer drives leukemogenesis in inv(3)(q21;q26) by activating EVI1 expression. *Cancer Cell*. 2014;25(4):415-427.

68. Gröschel S, Sanders MA, Hoogenboezem R, et al. A single oncogenic enhancer rearrangement causes concomitant EVI1 and GATA2 deregulation in leukemia. *Cell*. 2014;157(2):369-381.

69. Matharu N, Ahituv N. Minor Loops in Major Folds: Enhancer-Promoter Looping, Chromatin Restructuring, and Their Association with Transcriptional Regulation and Disease. *PLoS Genet*. 2015;11(12):e1005640.

70. Phanstiel DH, Boyle AP, Araya CL, Snyder MP. Sushi.R: flexible, quantitative and integrative genomic visualizations for publication-quality multi-panel figures. *Bioinformatics*. 2014;30(19):2808-2810.

Downloaded from http://ashpublications.net/blood/article-pdf/136/23/2679/1791833/bloodbld2020005394.pdf by guest on 02 June 2024